Earth and Planetary Science Letters 403 (2014) 188–198

Contents lists available at ScienceDirect

Earth and Planetary Science Letters

www.elsevier.com/locate/epsl

New crater calibrations for the lunar crater-age chronology

Stuart J. Robbins

Laboratory for Atmospheric and Space Physics, University of Colorado at Boulder, 3665 Discovery Dr., Boulder, CO 80309, United States

ARTICLE INFO

Article history:
Received 14 May 2013
Received in revised form 13 June 2014
Accepted 24 June 2014
Available online xxxx
Editor: C. Sotin

Keywords:
Moon
craters
lunar chronology
lunar history

ABSTRACT

Measuring the spatial density of craters emplaced on geologic units is the primary method used for remotely estimating ages of solar system surfaces. The calibration for this method, which enables conversion of crater density to absolute age, comes from *Apollo* and *Luna* lunar samples for which absolute radiometric ages have been determined. Researchers throughout the 1970s worked to establish the lunar chronology system based on that calibration, correlating crater densities with absolute ages. However, no uniform crater study has been conducted on all calibration terrains, a limitation that was previously unaddressed until this study. The latest lunar images from the *Lunar Reconnaissance Orbiter* were used here to re-map the eleven main sampling sites and new crater counts of those surfaces were conducted. These show significant differences for many sites' crater counts, in many cases having more craters than previously identified. These results, calibrated to the radiometric ages, show a revised lunar crater chronology that changes previously established crater-based ages by up about 1 billion years: Surfaces younger than ~3.6 Gyr and older than ~3.9 Gyr under the classic chronology are younger in this system, and those in-between are older in this new system.

1. Introduction

Craters are ubiquitous across nearly every solid surface in the solar system, and they have long been used as a metric for assigning relative ages: If a surface has more craters of a given size per unit area, then it is older because crater accumulation is temporally cumulative. Assigning absolute ages based on these crater counts requires calibrating a given crater density with a known surface age. Since the Moon represents a more ancient surface than Earth and *Apollo* astronauts and *Luna* craft returned samples that could be radiometrically dated, crater chronologies are based on the Moon. With such a model for the bombardment history at the Moon, one can use dynamical models for different bombardment rates of asteroids and comets on other planets to determine crater-based model ages across the rest of the inner solar system.

Almost all work upon which our current timescales are based was done in the 1970s using early satellite and *Apollo* photographs (Greeley and Gault, 1970; Shoemaker et al., 1970a, 1970b; Soderblom and Boyce, 1972; Neukum et al., 1975; Neukum and Horn, 1976; König, 1977; Moore et al., 1980; Neukum, 1983; Wilhelms, 1987; Neukum and Ivanov, 1994). Crater-based chronology is usually represented as the total number of craters with diameters $\geq$1 km per one or one million km^2 versus an absolute age; this crater density is denoted $N(1)$. The majority of age calibration points are from lunar mare (dark lava flood plains), two are from older lunar highlands, and five are tied to relatively young, individual craters, including three directly at the landing sites. These crater counts have been reexamined in part since recent imagery has been available and with a modern understanding of impactor dynamics, asteroid populations, and secondary cratering (Hartmann et al., 2007; Marchi et al., 2009; Hiesinger et al., 2012). The present study employs modern, uniform, high spatial resolution imagery to directly measure the $N(1)$ calibration points on surfaces of known ages that include $N(1)$ to perform the first uniform study of all calibration sites.

2. Methods

There have been no published geologic maps of the spacecraft landing sites since those from the *Apollo* Preliminary Science Reports (e.g., Shoemaker et al., 1969). These were based on early spacecraft, telescopic, and *Apollo* photographic data. Beyond these, other coarse maps were published that showed areas on which craters were measured (Greeley and Gault, 1970; Neukum et al., 1975), though the number of sites is limited in both; one recent study (Hiesinger et al., 2012) showed the small patches on which they identified craters. Consequently, the first step of this work was to examine the landing sites and map a single unit per site upon which craters could be identified, and all steps are summarized in Fig. 1.

E-mail address: stuart.robbins@colorado.edu.

http://dx.doi.org/10.1016/j.epsl.2014.06.038
0012-821X/

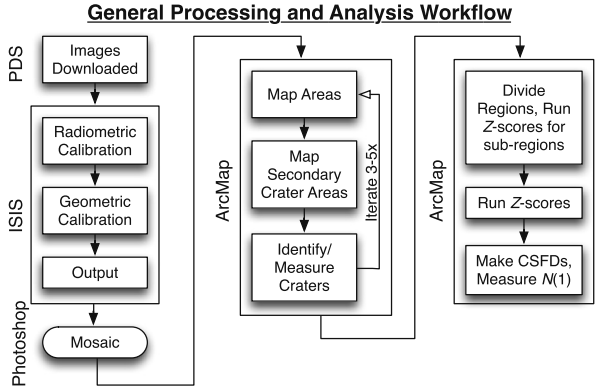

Fig. 1. Processing and analysis workflow (described in detail in Section 2). All images were downloaded from PDS and processed in ISIS. WAC images only were mosaicked in Photoshop. All mapping, crater identification, measurement was conducted in ArcMap, and then density and Z-statistic tests were run on each region and sub-regions within each region to verify they were homogeneous. Final analysis was conducted in Igor Pro software.

Images used were from the *Lunar Reconnaissance Orbiter* Camera Wide- and Narrow-Angle Camera (LROC WAC and NAC) obtained via the Planetary Data Systems (PDS) online interface, processed via standard techniques in Integrated Software for Imagers and Spectrometers (ISIS), and output in the lunar coordinate system. Images were taken at a solar incidence angle of ~58° and ~83° for all landing sites and WAC were manually assembled at a scaled 60 m/px in Adobe Photoshop to eliminate banding, lighting mismatches, and other artifacts that tend to result from automated mosaicking. While higher resolution imagery does exist for many sites, they were not used because the smallest features identified in this work were on the scale of ~500 m. NAC images were used for three small-crater calibration sites and were not mosaicked.

Mapping was conducted via standard geomorphologic techniques (Hare et al., 2009) with both imagery and topography data; an emphasis was placed on being conservative – eliminating any feature that could possibly be of a different unit or make crater identification more difficult (e.g., small massifs, graben, wrinkle ridges, rilles, large (>10 km) craters and associated ejecta). Unit boundaries were based on geologic contacts, linear geologic features, edges of mosaics, and lines of latitude or longitude to be roughly symmetric about the landing site (where applicable). Each mapped region was searched for morphologically distinct secondary craters which were also eliminated from the crater identification area; secondary craters were identified based on standard morphologic criteria (Shoemaker, 1962, 1965; Oberbeck and Morrison, 1974; McEwen and Bierhaus, 2006; Robbins and Hynek, 2014), but it is possible that non-morphologically obvious secondaries were not excluded (i.e., random background secondary craters that look like primary craters). The possibility of contamination by non-uniform random background secondary craters is discussed in the Supplementary material Section 2 and shown to be unlikely.

Accurate measurement of the area of mapped regions is important because crater counts are normalized to area. Areas were calculated in ArcMap via a Mollweide equal-area projection with false northing and central meridian at the center of each mapped region. The areas of regions of secondary craters were removed from the overall unit.

Craters with diameters $D \approx 0.5$–10 km were identified visually (manually) in the mosaics within the mapped regions and measured by tracing their rims, and the three youngest calibration points examined (Cone, North Ray, and South Ray craters) used craters as small as 10 m. The digitized rims were fit by a circle-fitting algorithm that calculates the location and diameter of the craters (Robbins and Hynek, 2012); included unpublished data by C.I. Fassett were measured on similar LROC images within ArcMap using the CraterTools software add-on (see Appendices A and B in Robbins et al., 2014). After this, all regions were arbitrarily sub-divided into two to four sub-regions. Crater density and a Z-statistic for each sub-region (and each overall region) were calculated to ensure uniformity (the same crater density as the overall region) and non-clustering. The Z-statistic is the number of standard deviations by which a Poisson distribution (which primary craters should follow) deviates from randomness and has been used to examine crater spatial distributions in the past (e.g., Clark and Evans, 1954; Squyres et al., 1997). In all cases in this study, the sub-region crater densities were within the uncertainty of the other sub-regions from the same site and the overall region itself, and the Z-statistic indicated that the null hypothesis – that the craters were spatially random – was not rejected.

In dating surfaces, the most common technique is to create a size-frequency distribution (SFD) which is a histogram of crater diameters (Crater Analysis Techniques Working Group, 1979). The histogram is summed from large to small diameters to create a cumulative version (CSFD), and this is divided by the area on which craters were identified. This was done for all sites, but instead of binning the CSFD, a ranked histogram was created so as to best represent the data. A ranked histogram is where craters are sorted from largest to smallest, the diameter placed on the abscissa, and the order in the list on the ordinate axis; this avoids the smoothing inherent in any binning system. The $N(1)$ data point was then read from the CSFDs in 7 of the 11 regions considered; in four cases, other techniques were used due to the small region mapped or empirical crater saturation at $D = 1$ km, discussed below. All sites' maps and CSFDs are shown in Figs. 3–5 (and high-resolution maps are included as online supplemental data). Three significant figures for the crater counts from this work are shown while others are listed to the precision found in the original papers.

3. Calibration sites

This section discusses each of the 11 calibration sites used with details of mapping, crater counts, and comparison with previous work. Figs. 3–5 show the mapping and crater counts. Three sites (*Apollo 15, 16*, and *Luna 24*) have historic maps available, and detailed comparisons are made in the supplemental material. Additional calibration details are also discussed in the supplemental material, including consistency tests to determine if secondary crater contamination was significant.

3.1. Apollo 11

Mare Tranquilitatis is ~6 million km^2, while the mapped region in this study around the lunar module *Eagle* is 13,892 km^2. The maria surrounding the lander appears homogenous with no obvious distinct units. The mapped region is bound by the limits of the WAC strips used to the north, the wrinkle ridge east of Sabine crater to the west, a series of grabens to the south, and a wrinkle ridge and 25.615° east (border of WAC strip); the region is roughly centered on Collins crater. This region is heavily contaminated by secondary craters and an area 1064 km^2 was removed to eliminate these, yielding a final area of 12,828 km^2. The results and literature comparisons are:

- $N(1) = 8140 \pm 800$ per 10^6 km^2 (this work)
- $N(1) = 4900 \pm 700$ (Fassett, pers. comm.)
- $N(1) = 9000 \pm 1800$ (Neukum and Ivanov, 1994)
- $N(1) = 9300$–9357 (Marchi et al., 2009, fitting data from Neukum, 1983)
- $N(1) \approx 9120$ (Shoemaker et al., 1970b)
- $N(1) \approx 12{,}900$ (Shoemaker et al., 1970a)

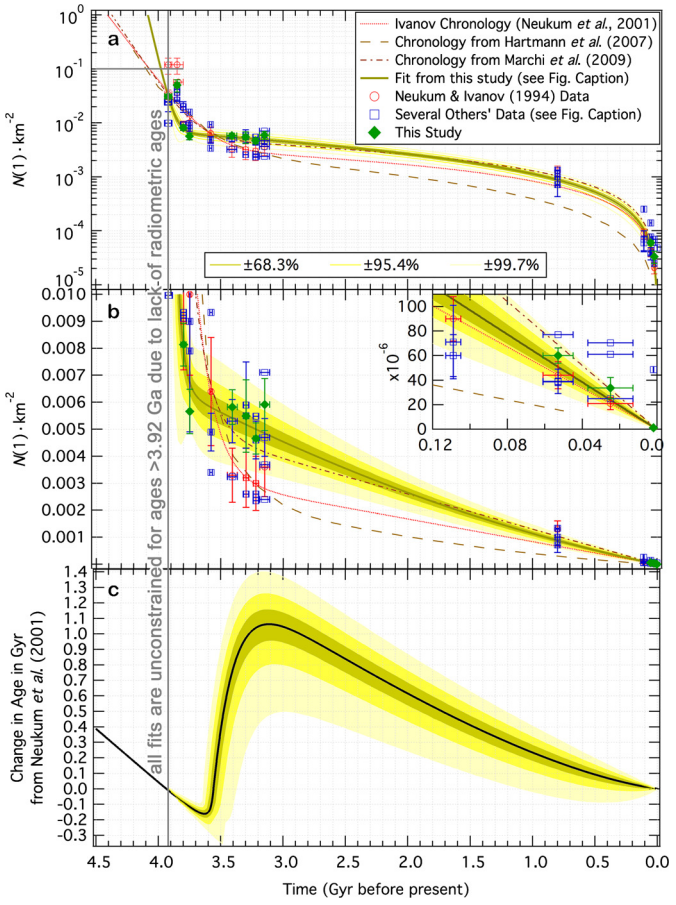

Fig. 2. The canonical chronology (Neukum et al., 2001) compared with revisions (Hartmann et al., 2007; Marchi et al., 2009) and this work are in panels a and b. Panel a shows the function on semi-log axes while Panel b focuses on the near-linear recent cratering rate on a linear scale with the last 120 Myr inset. Data originally used (Neukum, 1983) are displayed along with those from this study and several comparison works (Greeley and Gault, 1970; Shoemaker et al., 1970a; Soderblom and Boyce, 1972; Moore et al., 1980; Wilhelms, 1987; Marchi et al., 2009; Hiesinger et al., 2012; Fassett, pers. comm.). Panel c shows the difference between the new chronology and classic chronology (Neukum et al., 2001) as a function of age in the old chronology. 1σ, 2σ, and 3σ confidence bands to the fit from this work are overlaid. Lines at 3.92 Gyr and $N(1) = 10^{-1}$ indicate values greater than which the function should not be extrapolated due to lack of constraints.

- $N(1) = 3400$ for "young" terrain (Wilhelms, 1987)
- $N(1) = 6400 \pm 2000$ for "young" terrain (Neukum, 1983)

There is generally good agreement between this work and values for "old" *Apollo 11* terrain: Crater counts in early papers (e.g., Neukum et al., 1975) relied on crater counts in a different region of Mare Tranquillitatis by Greeley and Gault (1970) who found a near-saturated crater population (though they did not identify it as such) for diameters $D \lesssim 1$ km that had an $N(1) \approx 21{,}000 \pm 4600$, and a markedly different, shallower slope was found for $D \gtrsim 1$ km. This was interpreted as two different "young" and "old" surfaces near *Eagle*, and this interpretation has propagated throughout the literature since that time; it was even used by Stöffler and Ryder (2001) in their review work reassessing all lunar landing site radiometric ages to assign two ages – a "young" and "old" age – to the *Apollo 11* samples. However, these new crater counts are within 0.5σ of the Neukum production function (Neukum et al., 2001) for $0.8 < D < 6.0$ km, indicating only a single population. Since the $N(1)$ value from this work more closely matches that for historically "old" *Apollo 11* values, it is assumed that is what was measured.

3.2. Apollo 12

The *Apollo 12* lunar module *Intrepid* landed within Oceanus Procellarum approximately 400 km SSW of Copernicus crater. Despite its distance, it is still within the extensive ray system of Copernicus, and the landing site is heavily influenced by secondary craters both from Copernicus and the closer Reinhold and Lansberg craters. Other than these rays, the region surrounding the lander appears homogenous. The region in this work was defined as a 6510 km^2 area around the site, and 121 km^2 were removed as fields of secondary craters. The mapping region was bound by 2.0 °S to the north to avoid a large region of secondary craters; a prominent wrinkle ridge ~21.25 °W bound the region to the east and south, while a mountain range and ghost crater bound the region to the west. The results and literature comparisons are:

- $N(1) = 5910 \pm 960$ per 10^6 km^2 (this work)
- $N(1) = 4700 \pm 700$ (Fassett, pers. comm.)
- $N(1) = 2400 \pm 400$ (Wilhelms, 1987)
- $N(1) = 3600 \pm 1100$ (Neukum and Ivanov, 1994)
- $N(1) = 3683$–3695 (Marchi et al., 2009, fitting data from Neukum, 1983)
- $N(1) \approx 5100$ (Shoemaker et al., 1970b)
- $N(1) \approx 5000$ (Neukum and Horn, 1976)
- $N(1) = 4360 \pm 929$ (Neukum, 1983)

The measured $N(1)$ from this work is 2.5× that from Wilhelms (1987) of 2400 ± 400 and 1.6× that from Neukum and Ivanov (1994). It is possible that there were some unaccounted for secondary craters in this study, but that appears unlikely given the morphology and distribution of the craters identified (see Z-statistic discussion in Section 2). The result from this study is within the uncertainty of Shoemaker et al. (1970b), and their binned data overlaps well. Neukum (1983) directly measured $N(1)$, but then fit it to 83% the measured value. It is possible that the lower value was selected because they thought it represents the last resurfacing age (Neukum and Horn, 1976) where magma resurfaced craters $D < 1$ km, but a dichotomy of ages in the CSFD that they observed is not seen here.

3.3. Apollo 14

The *Antares* touched down in the Fra Mauro highlands, a formation that overlaps the ~80-km eponymous crater towards the southern margin, and one that is thought to be formed from ejecta from the formation of Imbrium. Cone crater, another key point in the chronology, is at the *Apollo 14* landing site. The highland formation was mapped conservatively here, such that only 1709 km^2 were included – the mountains themselves appeared to be one unit without clear differences to indicate multiple events. There was a small topography difference dividing the mapped region along a north-south line, but splitting the area along this revealed identical crater densities in both halves. Few distinct secondary crater chains were in this region, but 56 km^2 were excluded due to the presence of secondaries. This was one of the most difficult regions to identify craters upon because of its undulating appearance. Results and literature comparisons follow:

- $N(1) = 48{,}400 \pm 5400$ per 10^6 km^2 (this work via direct measurement)
- $N(1) = 25{,}000$–$48{,}000$ (Wilhelms, 1987)
- $N(1) = 37{,}000 \pm 7000$ (Neukum and Ivanov, 1994)
- $N(1) = 25{,}950$–$26{,}720$ (Marchi et al., 2009, fitting data from Neukum, 1983)
- $N(1) \approx 47{,}600$ (Soderblom and Boyce, 1972)
- $N(1) \approx 42{,}000$ (Swann et al., 1971)

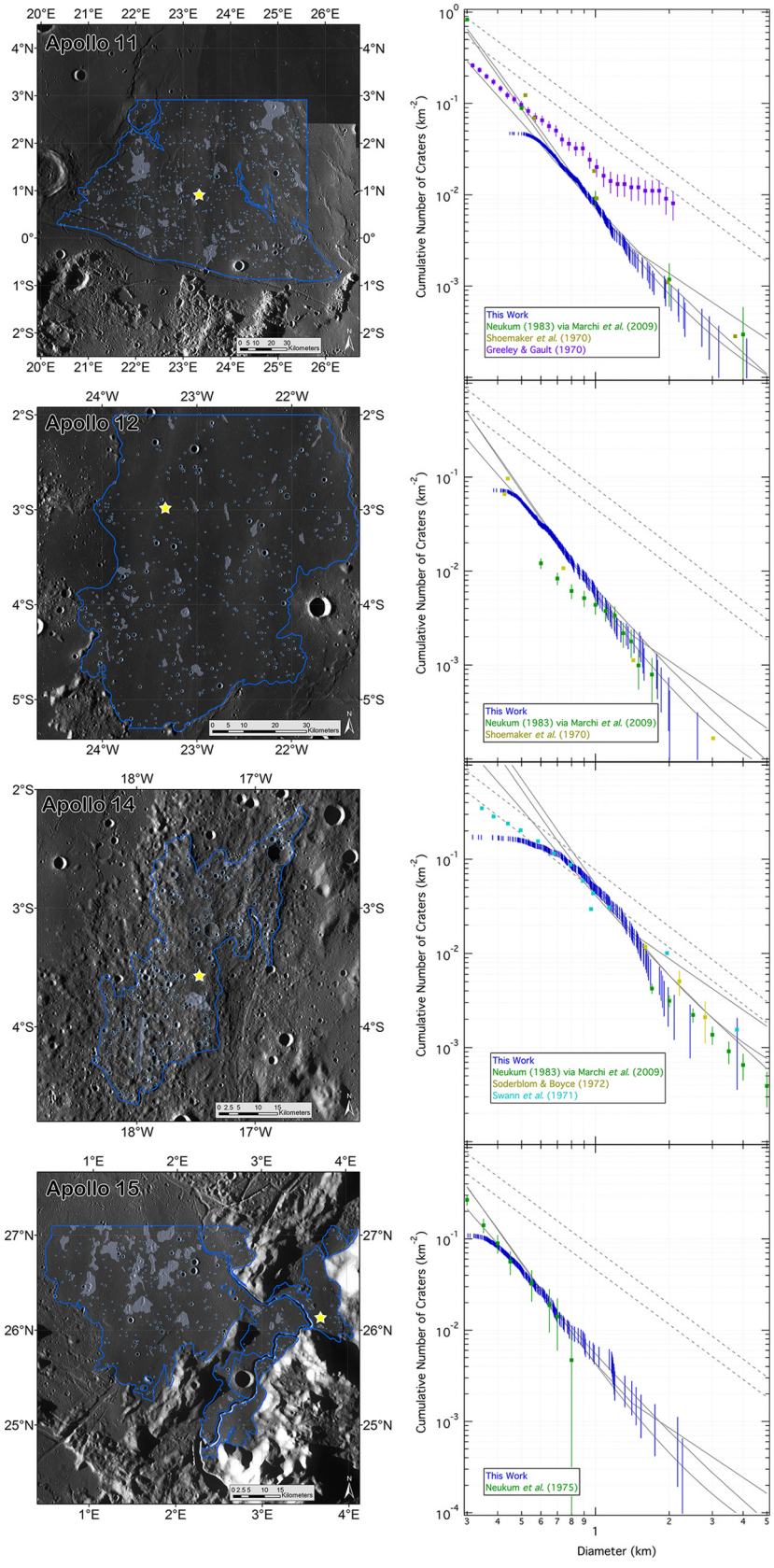

Fig. 3. Mapping (left column) and CSFDs with selected other work overlaid (right column). For each map, the area outlined in blue was the region upon which craters were identified, excluding pale blue regions which were identified as being clusters of secondary craters. A yellow star marks the location of each lander. In the right column, the CSFD for each region is shown with Poisson error bars on each point (Crater Analysis Techniques Working Group, 1979). The dashed lines indicate 3% and 5% of geometric saturation (Gault, 1970). The solid grey lines show Hartmann, Neukum, and Marchi et al. production functions (Neukum et al., 2001; Hartmann, 2005; Marchi et al., 2009) used to extrapolate the $N(1)$ point. Selected data from other works are overlaid if available. If possible, Neukum work (Neukum et al., 1975; Neukum, 1983) is kept as green (and turquoise) while others vary in color. Note: Colors refer to electronic version.

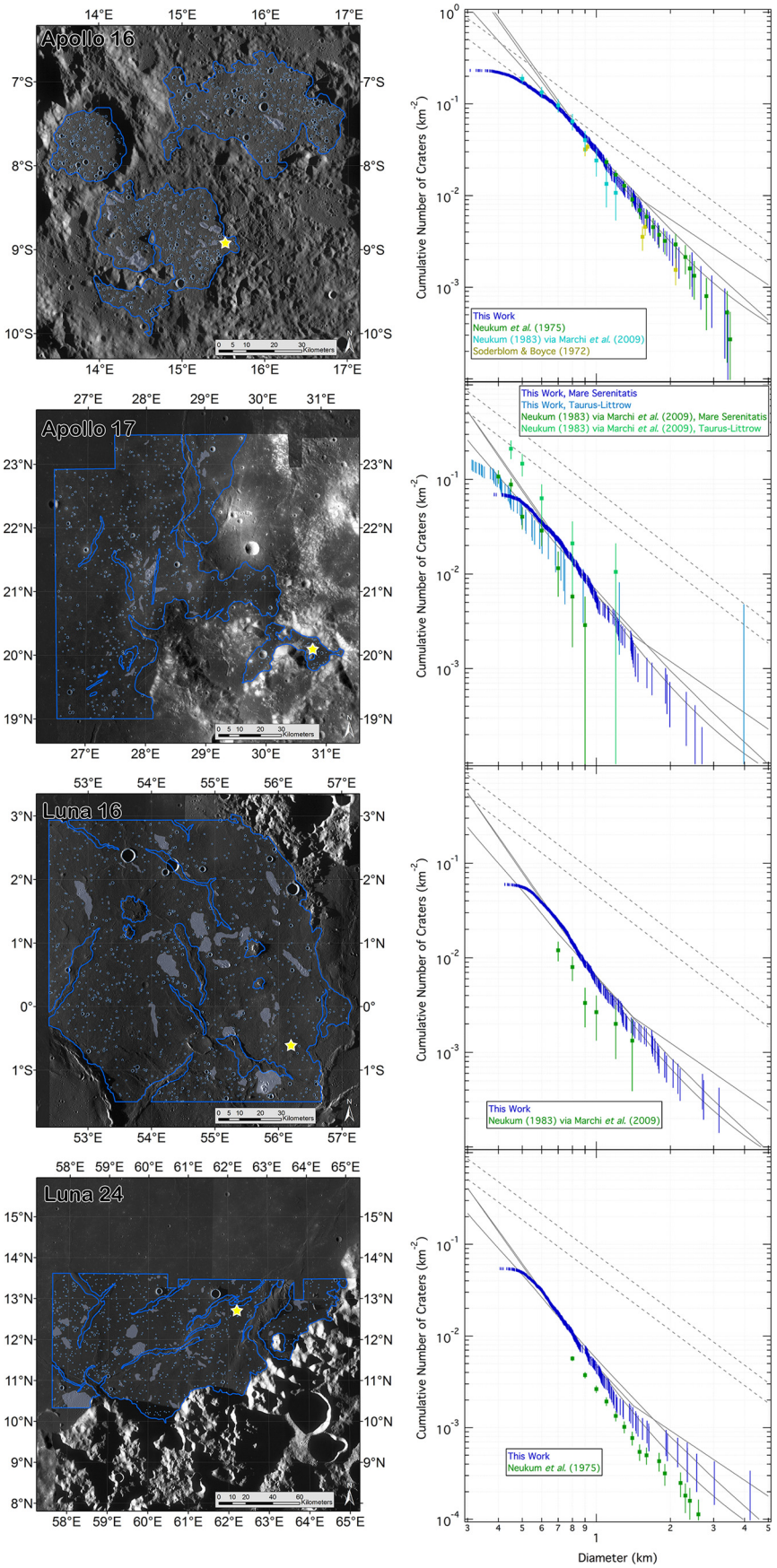

Fig. 4. See caption for Fig. 3.

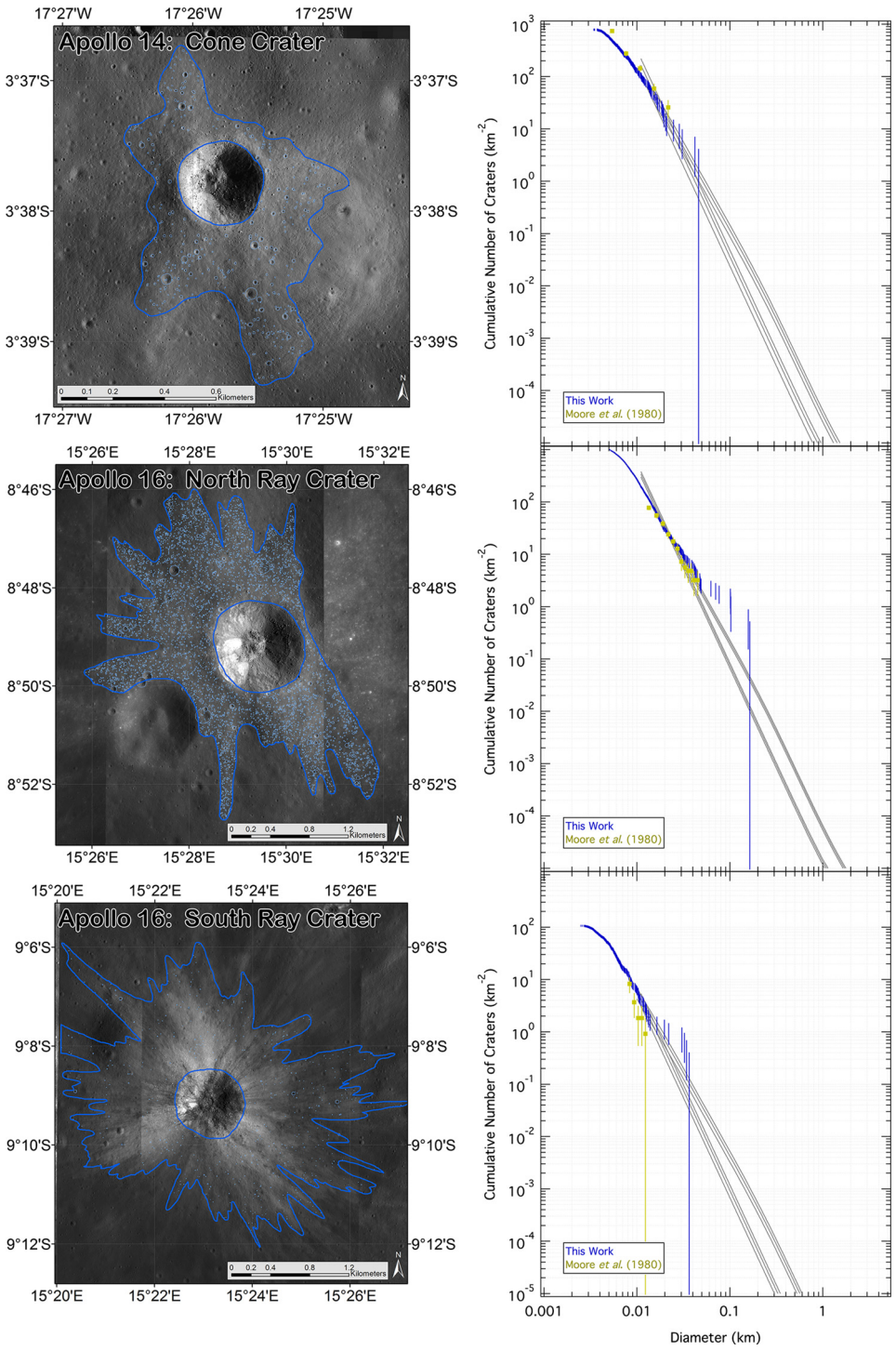

Fig. 5. See caption for Fig. 3. Differences are that the CSFDs axes' have changed and the Neukum and Hartmann production functions are shown in grey with three lines each, the middle being the best-fit and the two others indicating the uncertainty range. The increase in crater density above the isochrons for North and South Ray craters is likely due to several of the largest craters identified forming prior to the ejecta blanket but included accidentally in the counts; they were not used for fitting the isochrons.

The results overlap with some previous work, if being on the high end, but the *Antares* site is unique among other chronology sites in that it is empirically saturated for diameters $D < 1.3$ km at 3–4% of geometric saturation. This means that the measured $N(1)$ point is not useful, for no new information can be determined once the surface has empirically saturated with craters of that size. This saturation was unpublished by previous researchers, likely because the smallest diameters measured were ~1.7 km (Marchi et al., 2009, fitting data from Neukum, 1983) and ~1.6 km (Soderblom and Boyce, 1972); Swann et al. (1971) is a notable exception, but they do not provide a corrected $N(1)$ estimate. Binned data from Neukum (1983) do overlap this study except for their smallest point at $D = 1.7$ km.

A production function model (for lower density surfaces) is required to estimate an unsaturated value at $D = 1$ km. Unfortunately, the two most commonly used model production functions (Neukum et al., 2001; Hartmann, 2005) ("NPF" and "HPF" respectively) fail to match the slope for $1.3 < D < 4$ km of the Fra Mauro data presented here – the CSFD slope measured is steeper, potentially indicating some contamination by secondary craters, but as

per Section 2, the calculated Z-statistic indicates the data are not clustered, so any secondaries must be randomly strewn throughout if present. Regardless, attempting to fit to ~1.3–1.6 km with the HPF results in $N(1) \approx 44{,}800 \pm 8300$, fitting with NPF yields $N(1) \approx 55{,}300 \pm 10{,}400$, and fitting the MPF (from Marchi et al., 2009) yields $N(1) \approx 41{,}500 \pm 11{,}000$; since the NPF follows the crater distribution best and goes through $D_{max} \sim 2$ km, fitting the NPF results in $N(1) \approx 50{,}100 \pm 12{,}900$. One could use any of these extrapolations, the range, the NPF value which is the better fit, or not use the *Apollo 14* site at all – the implications for this are discussed in the supplemental material, though for this work, the NPF extrapolation through $D = 2$ km is used.

Finally, even though this is the most-densely cratered site examined in this work, it is not the oldest, for *Apollo 16* is dated to ~70 Myr older (Stöffler and Ryder, 2001). But, the crater counts at this site have almost always been found to be higher than at *Apollo 16* (Soderblom and Boyce, 1972; Wilhelms, 1987; Neukum and Ivanov, 1994).

3.4. Apollo 14, Cone crater

Cone crater, a 343-meter-diameter crater, was mapped in this work to ~0.5–1 crater diameters from the rim (crater cavity excluded). Crater counts were performed in this area of only 0.483 km^2 on LROC NAC images M114071006L and M162426054L (sun angles 57° and 76°, pixel scales ≈0.5 m/px); this is roughly twice the 0.272 km^2 area used previously (Moore et al., 1980). The largest crater of the 380 measured is only 46 meters across, and so an extrapolation must be performed to determine a model $N(1)$ value:

- $N(1) = 33.6 \pm 8.5$ per 10^6 km^2 (this work, NPF)
- $N(1) = 6.3 \pm 2.1$ (this work, HPF)
- $N(1) = 112 \pm 28$ (this work, MPF)
- $N(1) = 21 \pm 5$ (Neukum and Ivanov, 1994)
- $N(1) \approx 25$ (NPF extrapolation from Moore et al., 1980)
- $N(1) = 69.70$–71.31 (Marchi et al., 2009, fitting data from Moore et al., 1980)
- $N(1) = 61.2$ (Plescia and Robinson, 2011)

A cursory glance shows that these values differ by a factor of 18. The NPF extrapolation is used in fitting the new chronology function in this work because the NPF best follows the data, though this should be an area for future research.

3.5. Apollo 15

The *Falcon* lander touched down at the edge of Mare Imbrium to the east of Hadley Rille, roughly 150 km from the center of the prominent ~40-km-wide Autolycus crater. The mare unit appears homogenous on either side of the Rille, and so area both east and west of it was included in this work. Autolycus crater's ejecta and secondary crater streams dominate in the mare to the west of Hadley, and 301 km^2 of secondary craters were removed from the 3353 km^2 region mapped; a northern cut-off was set at 27.1° to avoid the heaviest areas of secondary cratering. This was also one of three sites where original mapped areas exist (Neukum et al., 1975) and compared (see supplemental material). The results and literature comparison are:

- $N(1) = 5500 \pm 1340$ per 10^6 km^2 (this work)
- $N(1) = 5900 \pm 1600$ (Fassett, pers. comm.)
- $N(1) = 2600$ (Wilhelms, 1987)
- $N(1) = 3200 \pm 1100$ (Neukum et al., 1975)
- $N(1) = 5468$–5526 (Marchi et al., 2009, fitting data from Neukum, 1983)

The results generally agree, and the raw data overlaps to within 0.25σ the binned data from Neukum et al. (1975), except for the largest point at $D = 0.8$ km; this point was rejected by Marchi et al. (2009) and including it would significantly lower a fitted density for $N(1)$.

3.6. Apollo 16

Apollo 16's lunar module *Orion* landed in the Cayley formation within the Descartes highlands between what was dubbed the "North Ray" and "South Ray" craters, two craters 1.0 and 0.7 km across, respectively. The site is complicated by geologic diversity, though this is one of three locations for which Neukum et al. (1975) provide a rough map of the areas in which they counted craters. The mapping approach adopted here is similar, only identifying craters on the relatively smooth Cayley formation and the floor of the large unnamed crater southeast of Lindsay. The total mapped areas were 1443 km^2 for the region that contains the *Orion* landing site, 1562 km^2 for the smooth region north-northeast of it, and 526 km^2 for the crater floor northwest of the site. 146 km^2 were removed in total due to secondary craters.

The results and literature comparisons are:

- $N(1) = 25{,}100 \pm 4200$ per 10^6 km^2 (this work, immediate site); $36{,}200 \pm 4800$ (this work, NNW region); $34{,}200 \pm 8100$ (this work, nearby crater floor)
- $N(1) = 31{,}000 \pm 3000$ (this work, final value combining all three regions)
- $N(1) = 26{,}000$ (Wilhelms, 1987)
- $N(1) = 34{,}000 \pm 7000$ (Neukum et al., 1975)
- $N(1) = 24{,}900$–$25{,}090$ (Marchi et al., 2009, fitting data from Neukum, 1983)
- $N(1) = 24{,}100 \pm 8040$ (Neukum, 1983)
- $N(1) \approx 22{,}241$ (Soderblom and Boyce, 1972)

It was not clear *a priori* if the three areas mapped were of the same unit, but once craters were identified, the three populations overlapped. Hence, they were combined for a final ensemble $N(1)$ density. When directly comparing original binned data from Neukum et al. (1975), their results are identical to within 0.3σ, though they only went as small as $D = 1.1$ km so the 1 km point was an extrapolation. Other data (Neukum, 1983) overlap within 1σ error bars. This site is important in contrast with *Apollo 14* which is usually radiometrically dated to be younger by 70–150 Myr (Stöffler and Ryder, 2001), but it has a much denser – and empirically saturated – crater population.

Ironically, the Cayley formation crater counts overlap the best with previous work and so they are the most certain in this study, but the radiometric age and origin of the material overprinted by craters is a topic of debate in the literature. The most recent review (Stöffler and Ryder, 2001) was used to remain consistent throughout this work. The implications of choosing different ages for this region are discussed in the online supplement's Section 4.

3.7. Apollo 16, North and South Ray craters

North Ray crater is another key point on the chronology curve. Mapping this crater was similar to Cone crater at the *Apollo 14* landing site: The area just interior to the crater rim was excluded while regions on the continuous ejecta up to ~1 crater diameter from the rim were included for a total area of 3.845 km^2, ~3× the area measured in Moore et al. (1980) and larger than Hiesinger et al. (2012) (this latter study had different mapping, choosing 2.12 km^2 in four polygonal areas around the crater, generally overlapping the mapping done here). NAC images M102064759R and M144524996L were used (sun angles 81° and 47°, pixel scales

Table 1
Summary data of *Apollo* and *Luna* site crater counts. $N(1)$ in the fourth column is the density of craters with diameters $D \geq 1$ km for each location normalized to 10^6 km^2, and uncertainty is the square-root of the number of craters also normalized to the area. Values are given to three significant figures.

Site	Area (km^2)	Craters	$N(1) \cdot 10^6$ km^{-2}	[a] $N(1) \cdot 10^6$ km^{-2}	[b] $N(1) \cdot 10^6$ km^{-2}	[c] $N(1) \cdot 10^6$ km^{-2}
Apollo 11	12,826	604	8140 ± 800	7030 ± 800	7670 ± 1020	7580 ± 950
Apollo 12	6389	463	5910 ± 960	5680 ± 690	5680 ± 740	6640 ± 790
Apollo 14	1653	285	$50{,}100 \pm 12{,}900$ [d]	$44{,}800 \pm 8300$	$50{,}100 \pm 12{,}900$	$41{,}500 \pm 11{,}000$
Cone Crater	0.483	380	33.6 ± 8.5 [e]	6.33 ± 2.14	33.6 ± 8.5	112 ± 28
Apollo 15	3052	332	5500 ± 1300	4340 ± 680	4280 ± 710	5530 ± 820
Apollo 16	3521	818	$31{,}000 \pm 3000$	$28{,}200 \pm 2700$	$29{,}600 \pm 3100$	$30{,}500 \pm 3000$
North Ray	3.845	4892	60.1 ± 6.3 [e]	13.2 ± 1.5	60.1 ± 6.3	203 ± 21
South Ray	4.947	527	1.23 ± 0.29 [e]	0.164 ± 0.045	1.23 ± 0.29	4.01 ± 0.94
Apollo 17, Serenitatis	8351	576	5660 ± 820	6090 ± 700	6140 ± 800	6770 ± 800
Apollo 17, Taurus Littrow	418.0	62	*not used*	3590 ± 850	3430 ± 810	5680 ± 1270
Luna 16	14,219	852	5820 ± 640	6440 ± 470	6430 ± 520	6260 ± 700
Luna 24	13,970	297	4660 ± 580	4760 ± 410	4760 ± 460	5660 ± 490

[a] Best fit of the $N(1)$-crossing data from this study when fitting crater data to the Hartmann (2005) production functions. Uncertainty is based on the uncertainty of the fit given Poisson error bars of the crater counts.
[b] Best fit of the $N(1)$-crossing data from this study when fitting crater data to the Neukum et al. (2001) production functions. Uncertainty is based on the uncertainty of the fit given Poisson error bars of the crater counts.
[c] Best fit of the $N(1)$-crossing data from this study when fitting crater data to the Marchi et al. (2009) production functions. Uncertainty is based on the uncertainty of the fit given Poisson error bars of the crater counts.
[d] Value is extrapolated from the NPF because the $N(1)$ point is saturated and NPF offers the best fit to the data; see text for more information.
[e] Values for the small crater calibration sites were extrapolated because $N(1)$ could not be directly measured. The NPF is used because it fits the data best and to be consistent; see text for more information.

1.0 and 0.5 m/px). The superposed craters do not reach the $D = 1.0$ km point and so extrapolation is required:

- $N(1) = 60.1 \pm 6.3$ per 10^6 km^2 (this work, NPF)
- $N(1) = 13.2 \pm 1.6$ (this work, HPF)
- $N(1) = 203 \pm 21$ (this work, MPF)
- $N(1) = 44 \pm 11$ (Neukum and Ivanov, 1994)
- $N(1) \approx 60$ (NPF extrapolation from Moore et al., 1980)
- $N(1) = 138.9$–142.1 (Marchi et al., 2009, fitting data from Moore et al., 1980)
- $N(1) = 77.2$ (Plescia and Robinson, 2011)
- $N(1) = 38.4$–39.0 (Hiesinger et al., 2012)
- $N(1) = 39 \pm 10$ (König, 1977)

The data fit the NPF remarkably well for $15 \leq D \leq 50$ m (NPF is only defined to $D \geq 15$ meters) so that is what is used in fitting a new chronology function. As with Cone crater, there is generally a large range of crater densities again spanning 15×, indicating that model-dependent results are highly variable. As an ensemble, the different values average 75, and the median is 60, indicating larger crater density outliers; the standard deviation is ±59, indicating there is little agreement in the literature. The raw data overlap very well with counts by Boyce (Moore et al., 1980) except their smallest bin at $D = 13$ m.

South Ray crater is a smaller, younger crater – the youngest on the usual chronology curve from lunar calibration samples at only $\sim 2 \pm 0.2$ Myr (Stöffler and Ryder, 2001). NAC image M181065865R (0.94 m/px, 68°) was used initially and craters were confirmed with M144524996R (0.43 m/px, 47°). Mapping and crater counting was done in the same manner as with North Ray over the extensive 4.95 km^2 ejecta, and $N(1) = 0.16 \pm 0.04$ was modeled from the HPF, 1.23 ± 0.29 from NPF, and 4.01 ± 0.94 from MPF. The raw data overlap the smallest two of five raw data points from Moore et al. (1980) – rising above the others – while the value from Plescia and Robinson (2011) is 48.7, significantly greater. This particular point is very difficult to estimate, not only because of self-secondary craters, boulder holes/trails, and buried craters within the ejecta blanket, but also because the largest superposed craters are ∼35 m in diameter, and the various PFs are only valid to $D_{\min}$ ∼11–15 m. For consistency with other extrapolated sites, the NPF fit is adopted.

3.8. Apollo 17

This location is typically cited as containing samples from three key chronology points: Mare Serenitatis, Taurus-Littrow valley, and Tycho crater. The landing itself was in the Taurus-Littrow valley within the Taurus mountain range and ∼50 km south of Littrow crater. The Taurus mountain range forms a southeastern margin of Mare Serenitatis. The Tycho point is indirect: a landslide in the valley is interpreted to have been caused by Tycho ejecta and cosmic ray exposure ages of the regolith at the site were used to date it (Stöffler and Ryder, 2001). Due to the indirect nature of this point, it was not used in this study.

The Taurus-Littrow valley was mapped with some parts west of the North and South Massifs that constrain the site. Ching-Te and Stella craters were included in this unit. The 58° sun angle WAC mosaic was used because the 84° sun angle caused half of the mapped region to be in shadow. Secondary crater contamination was not obvious except for the historically named "Central Cluster" that includes Camelot and Henry craters and immediately surrounds the lunar module *Challenger*; excluding it, only 418.0 km^2 were mapped.

- $N(1) = 5660 \pm 820$ per 10^6 km^2 (this work, Mare Serenitatis)
- $N(1) \approx 3510$ (this work, extrapolated for Taurus–Littrow)
- $N(1) = 7900 \pm 3000$ (Fassett, pers. comm.)
- $N(1) = 9000$ (Wilhelms, 1987)
- $N(1) = 10{,}000 \pm 3000$ (Neukum and Ivanov, 1994)
- $N(1) = 15{,}790$–$15{,}850$ (Marchi et al., 2009, fitting data from Neukum, 1983)

Direct measurement of the CSFD data through the 1 km point is $N(1) = 6400 \pm 3900$ per 10^6 km^2, but this value is based on only three craters and is anomalous in view of data at $D < 1$ km. Using the HPF, NPF, and MPF through diameters 0.38–0.75 km gives $N(1) = 3590 \pm 850$, 3430 ± 810, and 5680 ± 1270, respectively (the average is used in Table 1). These are roughly one-third the value quoted in Neukum and Ivanov (1994) and in Wilhelms (1987); the Marchi et al. (2009) fits to older data show crater densities also ∼3× greater than counts in this study. If they included the Central Cluster craters and extrapolated from smaller diameters, this would have significantly increased the number density.

However, these are not necessarily representative of the crater density on Mare Serenitatis. The entire mare was not mapped because of its large 360,000 km^2 area. Instead, the mapped region is bound by Brewster crater to the north, Borel crater to the west, Taurus mountains to the east, and extends south to the Robert, Mary, and Isis craters (19°N); this is an area of 8344 km^2. The outcrop on which Clerke crater sits was excluded along with the most prominent graben and wrinkle ridges. $N(1)/10^6 \cdot \text{km}^2 = 5660 \pm 820$.

This is still significantly smaller than the above-quoted values for Mare Serenitatis. Possible inclusion of the Clerke crater outcrop "lapping at the edges" of Mare Serenitatis in the original mapping from those works could explain this discrepancy. If that outcrop were the only region mapped, then $N(1) = 23{,}500 \pm 3700$ – over twice as large as historic values (and over four times as large as the other counts from this study). If the outcrop were included in the broader Mare Serenitatis area mapped, then $N(1) = 8740 \pm 930$, which is comparable with previous work, though that does not mean it is what should be used. Based on the Clerke crater mapping, the value of $N(1)/10^6 \cdot \text{km}^2 = 5660 \pm 820$ from the mare is used, without the outcrop containing Clerke crater.

3.9. Luna 16

The *Luna 16* craft returned 100 g of lunar material from the older Mare Fecunditatis region. The eastern part of the mare, where *Luna 16* landed, is heavily influenced by wrinkle ridges and the vast secondary crater field sourced from Langrenus crater, a 130-km-diameter crater ~250 km from the landing site. There is also an ancient ghost crater $D \approx 120$ km that forms the northeast part of the mare. To map this region, the mare around the site was included in this work while wrinkle ridges, the ghost crater, and a region within ~150 km of Langrenus crater were avoided (southern cut-off at 1.5°S). The total mapped area without secondary crater regions was 14,197 km^2, and the $N(1)$ values are:

- $N(1) = 5820 \pm 640$ per 10^6 km^2 (this work)
- $N(1) = 5300 \pm 800$ (Fassett, pers. comm.)
- $N(1) = 2660 \pm 1330$ (Neukum, 1983).
- $N(1) = 3300 \pm 1000$ (Neukum and Ivanov, 1994)
- $N(1) = 3234$–3257 (Marchi et al., 2009, fitting data from Neukum, 1983)

The $N(1)$ value from this work is larger than what has been previously reported (Neukum, 1983; Neukum and Ivanov, 1994; Marchi et al., 2009). However, more recent work by Fassett (pers. comm.) measured $N(1) = 5300 \pm 800$, supporting the larger value under modern imagery and mapping.

3.10. Luna 24

Luna 24 returned 170 g of lunar material from the relatively young Mare Crisium. The area in the south-southeastern mare immediately around the site was mapped. There are numerous wrinkle ridges running through the region, and though unlikely to affect the age, they were removed from the crater-mapping area. Along with the removal of regions with secondary craters, the total mapped area is 13,908 km^2.

- $N(1) = 4660 \pm 580$ (this work)
- $N(1) = 4600 \pm 700$ (Fassett, pers. comm.)
- $N(1) = 2600$ (Wilhelms, 1987)
- $N(1) = 2630 \pm 240$ (Neukum et al., 1975)
- $N(1) = 3000 \pm 600$ (Neukum and Ivanov, 1994)
- $N(1) = 2335$–2377 (Marchi et al., 2009, fitting data from Neukum, 1983)
- $N(1) \approx 5478$ (Soderblom and Boyce, 1972)

Despite this study finding a larger value than older work, the CSFDs overlap within reported error bars for $1.2 < D < 3$ km with data from Neukum et al. (1975); below and above this range, their data fall below this study, though this study's CSFD follows the NPF better to smaller diameters. The recent larger value is also supported by recent unpublished work by Fassett (pers. comm.), and further investigation (see online supplement) shows the discrepancy is likely due to Mare Crisium's non-uniform crater density.

3.11. Calibration site summary

As an ensemble, the 3.1–3.4 Ga sites (*Apollo 12, 15*, *Luna 16, 24*) are near the high end of $N(1)$ densities that have been reported previously, but in all cases except one, they are not the largest that have been published. The same is true for the oldest sites, *Apollo 14* and *16*; this means that a given terrain age corresponds to a larger crater density than was previously found. Conversely, the older *Apollo 11* (3.8 Ga) and 17 (3.75 Ga) sites were found to have the lowest $N(1)$ density when compared with the literature. These act to effectively "raise" the crater calibration curve – more craters are needed to reach a given age – while keeping the curve approximately linear over more of geologic history (Fig. 2).

For the few examples for which historic data are available (*Apollo 15, 16*, *Luna 24*), detailed comparisons were made (see supplemental material). From these, the main reasons that previous studies had different values are likely: (i) Earlier researchers did not always identify craters on the same unit as the landers, (ii) the $N(1)$ points were often extrapolated from larger or smaller craters based on models and not directly measured, (iii) the area occupied by secondary crater clusters was not excluded in previous work, and (iv) poor-quality images were sometimes used that limited the ability to identify craters.

4. Fitting a new chronology and conclusions

Once the maps and crater counts derived from *LRO* image data were completed, crater densities were correlated with absolute ages of lunar samples reported in the last major review (Stöffler and Ryder, 2001). The issue of deriving the lunar crater-age chronology is at least a three-part problem: craters, radiometric ages, and model production function. The purpose of this work was to address only that first part, which has generally languished in the literature. A comprehensive review of the second part is beyond the scope of this work, which is why the last major review is used, while I have endeavored to remain neutral on the model production function in this work.

After decades of analysis of the returned lunar samples, no sample has yet been tied to a geologic unit dated to either >3.92 Ga or ~1–3 Ga, so any fit is an extrapolation between ~1–3 Ga and is unconstrained for >3.92 Ga (Stöffler and Ryder, 2001) except by the total mass accreted by the Moon as indicated by the highly siderophile elements (Walker, 2009) and the total number of basins (Morbidelli et al., 2012). Over time, reasonable consensus has evolved that a function with an exponential decline for ages $\gtrsim$3.2 Ga and a linear rate thereafter adequately fit the data presently available (Neukum et al., 2001), even though there are likely to be numerous fits that may better represent the true cratering history.

The impact flux curve by Neukum et al. (2001) is what is used by most researchers today, and their chronology relating $N(1)$ and time T (in Gyr before present time) is of the form $N(1) = \alpha(\exp(\beta T) - 1) + \gamma T$ where, for the Moon, $\alpha = 5.44 \cdot 10^{-14}$, $\beta = 6.93$, and $\gamma = 8.38 \cdot 10^{-4}$. Complicating matters, Hartmann et al. (2007) proposed the classic time-scaling function be adjusted

Table 2
Parameters to fit the chronology function when using different data or extrapolations. The author recommends using the exponential-quadratic version with the "raw" data. Fits are of the form $N(1) = \alpha(\exp(\beta T) - 1) + \gamma T$ and $N(1) = \alpha(\exp(\beta T) - 1) + \gamma T + \delta T^2$.

	α	β	γ	δ
Original Data[a]	$9.83 \cdot 10^{-31}$	16.7	$1.19 \cdot 10^{-3}$	
Original Data[a]	$7.26 \cdot 10^{-41}$	22.6	$9.49 \cdot 10^{-4}$	$1.88 \cdot 10^{-4}$
HPF	*fit did not converge*			
HPF	$9.07 \cdot 10^{-53}$	29.6	$1.38 \cdot 10^{-4}$	$4.43 \cdot 10^{-4}$
NPF	$8.56 \cdot 10^{-32}$	17.3	$1.29 \cdot 10^{-3}$	
NPF	$6.61 \cdot 10^{-44}$	24.4	$9.45 \cdot 10^{-4}$	$2.00 \cdot 10^{-3}$
MPF	$6.36 \cdot 10^{-54}$	30.3	$1.93 \cdot 10^{-3}$	
MPF	$2.55 \cdot 10^{-38}$	21.1	$3.18 \cdot 10^{-3}$	$-4.20 \cdot 10^{-4}$

[a] "Original Data" refers to the raw counts discussed throughout this work except for the *Apollo 14*, and Cone, North Ray, and South Ray craters, where the NPF fits were used because they were the best fits to the data and for consistency.

to include a quadratic term that reflects a decrease in the cratering rate over the past few billion years: $N(1) = \alpha(\exp(\beta T) - 1) + \gamma T + \delta T^2$. The proposed model still matched the previous function for ages $T > 3$ Gyr, but it has a lower flux for younger surfaces.

Due to the limited sample sites and based on the $N(1)$ work in this study, there are many possible variations of data choice based on including or excluding certain data due to complications in mapping, measuring craters on the units, and the uncertainty in age (see supplemental material). Besides this, there is a natural variability in not only basic crater identification (Robbins et al., 2014), but the inherent Poisson uncertainties on the $N(1)$ counts range from ±10–26% (average ±14%) relative to the value, which raises additional uncertainty in any fit (Campbell, 1999). In the end, both the linear and the quadratic forms of the fit function were fit to the data, and the data were weighted by the Poisson counting uncertainties and confidence intervals were calculated. These are used in lieu of attempting a different function because of historical context and there are not enough data at this time to say that an early exponential decline followed by a linear or quadratic cratering rate afterwards is not a reasonable approximation to the data available. These functions were both fit with the observed $N(1)$ densities discussed in the text and fitted values from the HPF, NPF, and MPF (Table 1). The fit coefficients are in Table 2.

The Akaike and Bayesian Information Criteria (AIC, BIC) tests (Akaike, 1974; Schwarz, 1978) can be used to determine the relative goodness of highly non-linear fits such as these, and whether one is statistically better than the other or if it appears better but that is due to increasing the number of fit parameters. Both accomplish this by penalizing the indicator for increasing the number of fit parameters, but both showed that the Hartmann variation was a statistically better fit for all cases (observed $N(1)$ density and all three PF fits), and the AIC and BIC showed (as a control) that when adding a cubic term, the fit was statistically weaker – the amount of improvement of the fit did not compensate for the addition of another free parameter. The final fit parameters when using the observed data are $\alpha = 7.26 \cdot 10^{-41}$, $\beta = 22.6$, $\gamma = 9.49 \cdot 10^{-4}$, and $\delta = 1.88 \cdot 10^{-4}$ (Table 2). The formal 3σ uncertainty of this fit is ±30–40% in age, varying as a function of T (Fig. 2c). The data from Table 1 are displayed in Fig. 2 with this fit and several published chronology functions. While all calibration sites drive this difference from Neukum et al. (2001) except for *Apollo 16*, the points that effect the largest difference are the lower crater density at *Apollo 17* and higher density for *Apollo 12, 15*, *Luna 16*, and *24*.

The qualitative consequences of this new chronology, in comparison with the established Neukum et al. (2001) fit, are primarily three-fold: First, the much smaller α parameter indicates the formerly linear term, now quadratic, dominates over more of geologic time; instead of the exponential dominating for $T > 3.2$ Ga, its effect is $T > 3.7$ Ga, and it is mainly present due to the much larger spatial crater density at the *Apollo 14* and *16* sites. Second, the larger β term increases the exponential significantly, i.e., the cratering rate increases very quickly as one moves further into the past, at least for as long as the data are valid ($T \leq 3.92$ Ga); a potential solution to the run-away exponential is to introduce a sawtooth-like discontinuity around 4 Ga (Morbidelli et al., 2012). Third, there are two points of intersection – 3.6 and 3.9 Ga – where surfaces would have the same age under both chronologies at both corresponding crater densities. Between those two ages, surfaces of a given crater density are older by up to ~150 Myr. Surfaces previously dated as younger than 3.6 Ga are pushed younger by a maximum of 1.1 Gyr for those were previously dated to 3.1 Ga. This has broad implications for processes thought to occur ~2–3.5 Ga, such as continued volcanic activity on the Moon – these processes that had previously been age-modeled via crater counts likely occurred up to 1 Gyr more recently than previously thought. In the other chronological direction, the chronology is again unconstrained for ages >3.92 Ga, and so no inferences can be made about the likelihood of the Late Heavy Bombardment.

An important constraint and lunar point of interest is the age of Copernicus crater. It was not used in the chronology in this work because it has an indirectly determined absolute age and may or may not be represented in the sample collection. Fitting the new chronology to recent crater counts by Hiesinger et al. (2012) who measured $N(1) \cdot 10^6 = 435$–1010, the superposed crater density's model age, 400–860 Myr, overlaps its generally accepted radiometric age of 800 ± 15 Myr (Stöffler and Ryder, 2001). Also, Tycho crater has been dated to 109 ± 4 Ma, and Hiesinger et al. (2012) found a superposed density of $N(1) \cdot 10^6 \approx 30$–$100$; the model age in this chronology is 30–95 Myr, a little younger than the accepted radiometric age, though it is within the 1σ confidence band from the fit.

This work, based on a new generation of uniform and high spatial resolution lunar images, performed in a uniform manner, and including craters that cover the critical $D = 1$ km calibration point, should be the most accurate crater calibration dataset to-date. Since crater size–frequency distributions of the regions for which we have lunar samples have been used for decades to extrapolate the lunar chronology function to all other inner solar system planets and sometimes to the outer solar system (e.g., Neukum, 1983; Tanaka, 1986; Phillips et al., 1992; Nimmo and McKenzie, 1998; Neukum et al., 2001; Basilevsky and Head, 2003; Dones et al., 2009; Marchi et al., 2009), the implications of this revised chronology are far-reaching: It provides an enhanced calibration of the lunar cratering flux for use when assigning model crater-based ages to terrestrial planetary surfaces.

Acknowledgements

Support for Robbins was made possible through the Maryland Space Grant Consortium and the NASA Lunar Science Institute Central office through CosmoQuest's "Moon Mappers" project. Thanks to S. Marchi for providing original Neukum crater count data from the *Apollo* landing sites. Thanks to C.I. Fassett for providing unpublished data for comparison. Thanks to E.B. Bierhaus, W.F. Bottke, C.R. Chapman, B.M. Hynek, and M. Norman for discussions; J.M. Boyce and C.R. Chapman for help locating older manuscripts; and W.F. Bottke, J.M. Boyce, C.R. Chapman, L. Dones, C.I. Fassett, B.M. Hynek, and J. Robbins for feedback on early drafts. Thanks to E.B. Bierhaus and S. Marchi for their reviews. *Apollo* metric camera images are © NASA/JSC/Arizona State University.

Appendix A. Supplementary material

Supplementary material related to this article can be found online at http://dx.doi.org/10.1016/j.epsl.2014.06.038.

References

Akaike, H., 1974. A new look at the statistical model identification. IEEE Trans. Autom. Control 16 (6), 716–723. http://dx.doi.org/10.1109/TAC.1974.1100705.

Basilevsky, A.T., Head, J.W., 2003. The surface of Venus. Rep. Prog. Phys. 66, 1699–1734. http://dx.doi.org/10.1088/0034-4885/66/10/R04.

Campbell, B.A., 1999. Surface formation rates and impact crater densities on Venus. J. Geophys. Res. 104 (E9), 21,951–21,955. http://dx.doi.org/10.1029/1998JE000607.

Clark, P.J., Evans, F.C., 1954. Distances to nearest neighbor as a measure of spatial relationships in populations. Ecology 35, 445–453.

Crater Analysis Techniques Working Group, 1979. Standard techniques for presentation and analysis of crater size–frequency data. Icarus 37, 467–474. http://dx.doi.org/10.1016/0019-1035(79)90009-5.

Dones, L., et al., 2009. Icy satellites of Saturn: impact cratering and age determination. In: Dougherty, M., Esposito, L., Krimigis, S. (Eds.), Saturn from Cassini–Huygens. Springer, ISBN 978-1402092169.

Gault, D.E., 1970. Saturation and equilibrium conditions for impact cratering on the Lunar surface: criteria and implications. Radio Sci. 5 (2), 273–291. http://dx.doi.org/10.1029/RS005i002p00273.

Greeley, R., Gault, D.E., 1970. Precision size–frequency distributions of craters for 12 selected areas of the lunar surface. Moon 2, 10–77. http://dx.doi.org/10.1007/BF00561875.

Hare, T.M., Skinner Jr., J.A., Tanaka, K.L., Fortezzo, C.M., Bleamaster III, L.F., Sucharski, R.M., 2009. GIS-based planetary geologic maps: recommendations for improved preparation, review, and publication. In: 40th Lunar & Planet. Sci. Conf. The Woodlands, TX, 23–27 March 2009. Abstract #2538.

Hartmann, W.K., 2005. Martian cratering 8: isochron refinement and the chronology of Mars. Icarus 174, 294–320. http://dx.doi.org/10.1016/j.icarus.2004.11.023.

Hartmann, W.K., Quantin, C., Mangold, N., 2007. Possible long-term decline in impact rates 2. Lunar impact-melt data regarding impact history. Icarus 186, 11–23. http://dx.doi.org/10.1016/j.icarus.2006.09.009.

Hiesinger, H., van der Bogert, C.H., Pasckert, J.H., Funcke, L., Giacomini, L., Ostrach, L.R., Robinson, M.S., 2012. How old are young lunar craters? J. Geophys. Res. 117. http://dx.doi.org/10.1029/2011JE003935. CiteID E00H10.

König, B., 1977. Untersuch. von Primaren und Sekundaeren Einschlagstrukturen auf dem Mond und Labexperimente zum Studium des Auswurfs von Sekundaerteilchen. Thesis. Heidelberg University.

Marchi, S., Mottola, S., Cremonese, G., Massironi, M., Martellato, E., 2009. A new chronology for the Moon and Mercury. Astron. J. 137 (6), 4936–4948. http://dx.doi.org/10.1088/0004-6256/137/6/4936.

McEwen, A.S., Bierhaus, E.B., 2006. The importance of secondary cratering to age constraints on planetary surfaces. Annu. Rev. Earth Planet. Sci. 34, 535–567. http://dx.doi.org/10.1146/annurev.earth.34.031405.125018.

Moore, H.J., Boyce, J.M., Hahn, D.A., 1980. Small impact craters in the lunar regolith – their morphologies, relative ages, and rates of formation. Moon Planets 23, 231–252. http://dx.doi.org/10.1009/BF00899820.

Morbidelli, A., Marchi, S., Bottke, W.F., Kring, D.A., 2012. A sawtooth-like timeline for the first billion years of lunar bombardment. Earth Planet. Sci. Lett. 355–356, 144–151. http://dx.doi.org/10.1016/j.epsl.2012.07.037.

Neukum, G., 1983. Meteoritenbombardement und Datierung planetarer Oberflachen. Habilitation thesis. University of Munich.

Neukum, G., Horn, P., 1976. Effects of lava flows on lunar crater populations. Moon 15, 205–222. http://dx.doi.org/10.1007/BF00562238.

Neukum, G., Ivanov, B.A., 1994. Crater size distributions and impact probabilities on Earth from lunar, terrestrial-planet, and asteroid cratering data. In: Gehrels, T., Matthews, M.S., Schumann, A.M. (Eds.), Hazards due to comets and asteroids. University of Arizona Press, ISBN 978-0816515059. 359 pp.

Neukum, G., König, B., Arkani-Hamed, J., 1975. A study of lunar impact crater size-distributions. Moon 12, 201–229. http://dx.doi.org/10.1007/BF00577878.

Neukum, G., Ivanov, B.A., Hartmann, W.K., 2001. Cratering records in the inner solar system in relation to the lunar reference system. In: Chronology and Evolution of Mars. Space Sci. Rev. 96, 55–86.

Nimmo, F., McKenzie, D., 1998. Volcanism and tectonics on Venus. Annu. Rev. Earth Planet. Sci. 26, 23–51. http://dx.doi.org/10.1146/annurev.earth.26.1.23.

Oberbeck, V.R., Morrison, R.H., 1974. Laboratory simulation of the herringbone pattern associated with lunar secondary crater chains. Moon 9, 415–455. http://dx.doi.org/10.1007/BF00562581.

Phillips, R.J., Raubertas, R.F., Arvidson, R.E., Sarkar, I.C., Herrick, R.R., Izenberg, N., Grimm, R.E., 1992. Impact craters and Venus resurfacing history. J. Geophys. Res. 97 (E10), 15,923–15,948. http://dx.doi.org/10.1029/92JE01696.

Plescia, J.B., Robinson, M.S., 2011. New Constraints on the Absolute Lunar Crater Chronology. In: 42nd Lunar & Planet. Sci. Conf. The Woodlands, TX, 7–11 March 2011. Abstract #1839.

Robbins, S.J., Hynek, B.M., 2012. A new global database of Mars impact craters $\geq$1 km: 1. Database creation, properties, and parameters. J. Geophys. Res. 117. http://dx.doi.org/10.1029/2011JE3966. CiteID E05004.

Robbins, S.J., Hynek, B.M., 2014. The secondary crater population of Mars. Earth Planet. Sci. Lett. 400, 66–76. http://dx.doi.org/10.1016/j.epsl.2014.05.005.

Robbins, S.J., et al., 2014. The variability of crater identification among expert and community crater analysts. Icarus 234, 109–131. http://dx.doi.org/10.1016/j.icarus.2014.02.022.

Schwarz, G.E., 1978. Estimating the dimension of a model. Ann. Stat. 6 (2), 461–464. http://dx.doi.org/10.1214/aos/1176344136.

Shoemaker, E.M., 1962. Interpretation of lunar craters. In: Kopal, Z. (Ed.), Physics and Astronomy of the Moon. Academic Press, New York.

Shoemaker, E.M., 1965. Preliminary analysis of the fine structure of the lunar surface. In: Heiss, W.N., Menzel, D.R., O'Keefe, J.A. (Eds.), Mare Cognitum, in The Nature of the Lunar Surface. Johns Hopkins Univ. Press, Baltimore, MD.

Shoemaker, E.M., et al., 1969. Geologic setting of the lunar samples returned by the *Apollo 11* mission. In: *Apollo 11* Preliminary Science Report. NASA, Washington, DC, pp. 41–84.

Shoemaker, E.M., Hait, M.H., Swann, G.A., Schleicher, D.L., Dahlem, D.H., Schaber, G.G., Sutton, R.L., 1970a. Tranquility base. Science 167 (3918), 452–455. http://dx.doi.org/10.1126/science.167.3918.452.

Shoemaker, E.M., et al., 1970b. Preliminary geologic investigation of the *Apollo 12* landing site: Part A. Geology of the *Apollo 12* landing site. In: *Apollo 12* Preliminary Science Report. NASA, Washington, DC, pp. 113–156.

Soderblom, L.A., Boyce, J.M., 1972. Photogeology: Part A. Relative ages of some near-side and far-side terra plains based on *Apollo 16* metric photography. In: *Apollo 16* Preliminary Science Report. NASA, Washington, DC, pp. 29-3–29-8.

Squyres, S.W., Howell, C., Liu, M.C., Lissauer, J.J., 1997. Investigation of crater "saturation" using spatial statistics. Icarus 125, 67–82. http://dx.doi.org/10.1006/icar.1996.5560.

Stöffler, D., Ryder, G., 2001. Stratigraphy and isotope ages of lunar geologic units: chronological standard for the inner solar system. Space Sci. Rev. 96, 9–54.

Swann, G.A., et al., 1971. Preliminary geologic investigations of the *Apollo 14* landing site. In: *Apollo 14* Preliminary Science Report. NASA, Washington, DC, pp. 39–86.

Tanaka, K.L., 1986. The stratigraphy of Mars. J. Geophys. Res. 91: B13, E139–E158. http://dx.doi.org/10.1029/JB091iB13p0E139.

Walker, R.J., 2009. Highly siderophile elements in the Earth, Moon and Mars: update and implications for planetary accretion and differentiation. Chem. Erde Geochem. 69 (2), 101–125. http://dx.doi.org/10.1016/j.chemer.2008.10.001.

Wilhelms, D.E., 1987. The Geologic History of the Moon. USGS Prof. Paper 1348.